JOURNAL OF SOLID STATE CHEMISTRY 93, 193–201 (1991)

β-MoO_3 Produced from a Novel Freeze Drying Route

J. B. PARISE

Mineral Physics Institute and Department of Earth and Space Sciences, State University of New York, Stony Brook, New York 11794-2100

E. M. McCARRON III

Central Research and Development Department, E. I. Dupont de Nemours & Co., Inc., Experimental Station, P.O. Box 80356, Wilmington, Delaware 19880-0356

AND R. VON DREELE AND J. A. GOLDSTONE

Manual Lujan Jr. Neutron Scattering Center (LANSCE), Los Alamos National Laboratory, Los Alamos, New Mexico 87545

Received December 21, 1990; in revised form March 18, 1991

Powdered samples of β-MoO_3 have been produced by the gentle heat treatment of freeze-dried molybdic acid at 350°C for 1 hr. The samples, yellow-green in appearance, contained varying amounts of the thermodynamically stable α-MoO_3, depending upon the time and temperature of heat treatment. Neutron diffraction data were collected at 300 K. All peaks, not attributable to α-MoO_3, were indexed on the basis of a monoclinic cell, $P2_1/c$, $a = 7.1228(7)$, $b = 5.3660(6)$, $c = 5.5665(6)$, $\beta = 92.01(1)°$, $V = 212.62(6)$ Å^3. The structure, which is related to ReO_3, contains two crystallographically independent octahedra. Both show evidence of disorder at the Mo and O sites. Two distinct orientations of a short Mo–O distance, suggestive of the type of molybdenyl bond observed in both the α and β'-forms, are primarily responsible for the observed disordering.

1. Introduction

The thermodynamically stable oxides of the group VIB metals, with oxidation state VI, crystallize in three distinct structure types. The structure of CrO_3 consists of independent chains of corner-linked tetrahedra (*1*), while that of α-MoO_3 (*1*), depicted in Fig. 1, is layered, containing edge- and corner-linked octahedra. The structure of WO_3, also shown in Fig. 1, consists of a network of corner-connected octahedra and is related to the ReO_3 structure type (*1*).

Recently, two new forms of molybdenum trioxide, both structurally related to WO_3 (Fig. 1) rather than to α-MoO_3, have been reported (*2, 3*). The first of these, designated β-MoO_3 by McCarron (*2*), was synthesized by gently heating spray-dried molybdic acid, which had been produced by passing sodium molybdate over an ion-exchange resin. Using evidence such as similarities in their Raman spectra, a structural relationship was inferred between the β-phase and WO_3. Yet another novel form of MoO_3, designated β'-MoO_3 (*3*), was produced when

0022-4596/91 $3.00

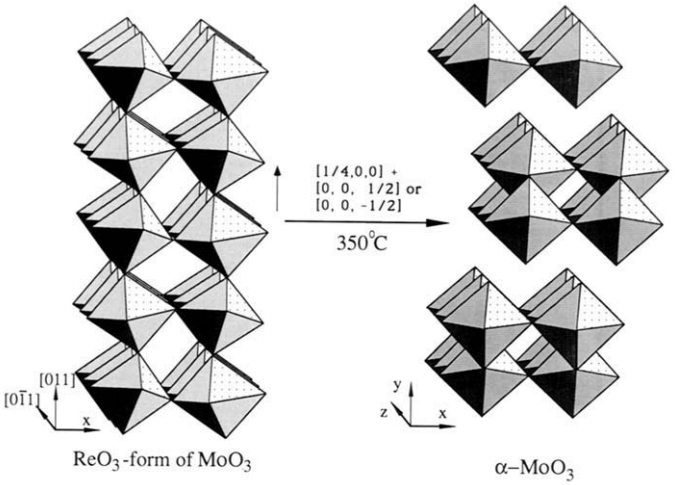

FIG. 1. A comparison of the structures of the ReO_3-related and α-forms of MoO_3. The displacements, in terms of the unit cell of β-MoO_3, required to transform from the β- to the α-form are given (see text).

hydrogen was removed from a bronze formed by treating β-MoO_3 in a hydrogen spillover reaction (*3*). The structures of β′-MoO_3 and H_xMoO_3, which were refined using powder neutron diffraction data, are depicted in Fig. 2. They are closely related to that of a monoclinic form of WO_3, with Mo atoms octahedrally coordinated to oxygen and all octahedra corner-linked to form an open framework.

On the other hand, a confirmation of the structure of β-MoO_3 has not been forthcoming, even though its synthesis has been reported from other than the spray drying route (*4*). Despite evidence (*2*) supporting a structural relationship between the β-phase and WO_3, we were unable to obtain satisfactory structural refinements from samples prepared via the spray-dried route. Frustration at our inability to deal with this seemingly trivial structure led us to seek an alternate route to its synthesis in the hope that more suitable materials might be obtained. We report here a new synthetic route to β-MoO_3, and confirmation of its close structural relationship to WO_3 and ReO_3.

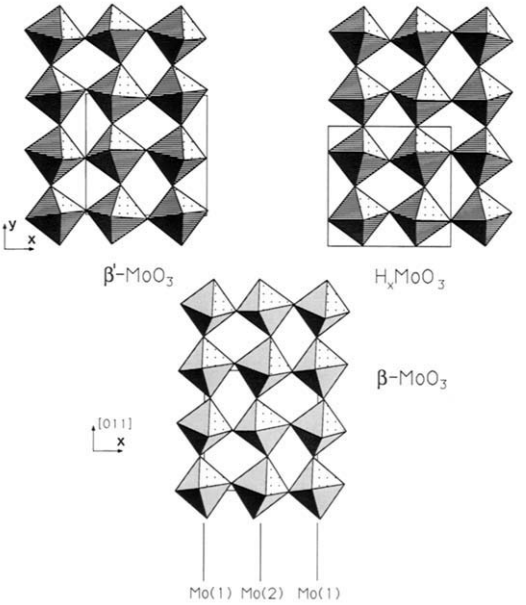

FIG. 2. Relationship between one layer of octahedra for β′-MoO_3, H_xMoO_3, and β-MoO_3, projected along [001], [00$\bar{1}$], and [011], respectively. For β′-MoO_3, the Mo(2) and O atoms have been placed on their ideal positions; see text and Table I for details.

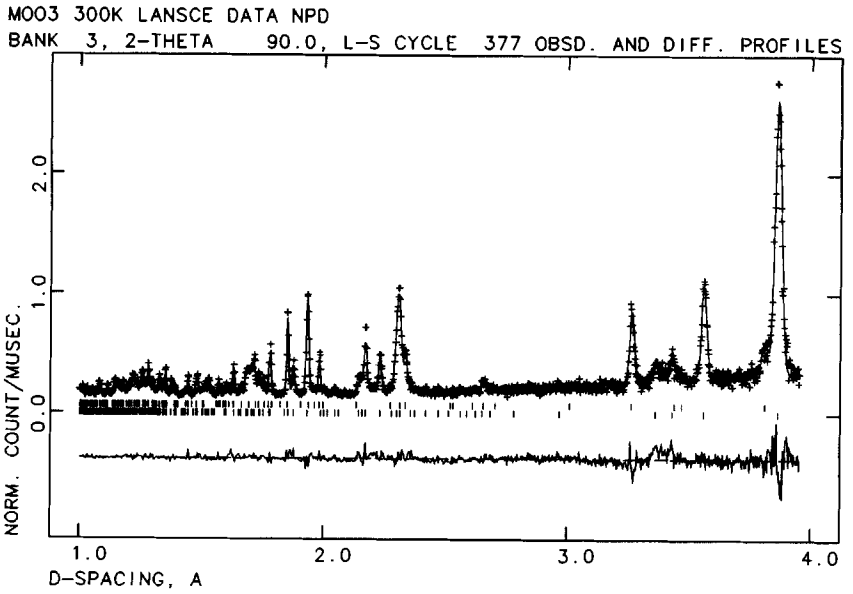

FIG. 3. Part of the neutron diffraction data for β-MoO_3 taken on the NPD at LANSCE. Data shown as plus (+) marks represent data collected on the 90° data bank at 300 K. The continuous line is the calculated profile from Rietveld refinement (Table I). The sets of tick marks below the data indicate the positions of allowed reflections from β-MoO_3 (bottom) and α-MoO_3. The lower curve is the difference between observed and calculated profiles plotted on the same scale as the observed data.

2. Experimental

2.1. Synthesis and Characterization

A sample β-MoO_3 was obtained in the following manner: An aqueous solution of $Na_2MoO_4 \cdot 2H_2O$ (25 g in 100 ml, pH ~9) was passed over a cation-exchange resin, Rexyn 101 (H). In addition to the pH, the sodium content was monitored with a sodium selective electrode. The pH of the final solution was determined to be ~1.7 and the sodium content less than 10^{-3} *M*. The molybdic acid solution was frozen by atomization into liquid nitrogen and subsequent sublimation using a commercial freeze drying apparatus. The resulting powder, pale green in color, was reminiscent of powder produced by spray drying techniques (5). The composition of this powder, as determined by thermogravimetric analysis, was $MoO_3 \cdot 1.5\ H_2O$. The measured surface area was 14.1 m^2/g. Heat treatment of this amorphous powder, at 300°C for 1 h in flowing oxygen, produced crystalline β-MoO_3. Unfortunately α-MoO_3, the thermodynamically stable phase, was also present in all preparations. Freshly prepared β-MoO_3 had a yellow coloration.

2.2. Data Collection

A 5-g sample of freshly prepared sample containing 85 mole% β-MoO_3 (see below) was packed into a standard vanadium holder and neutron powder diffraction data were taken at 300 K on the neutron powder diffractometer (NPD) at the Manual Lujan Jr., Neutron Scattering Center (LANSCE) at the Los Alamos National Laboratory. The NDP has a flight path of 32 m and a resolu-

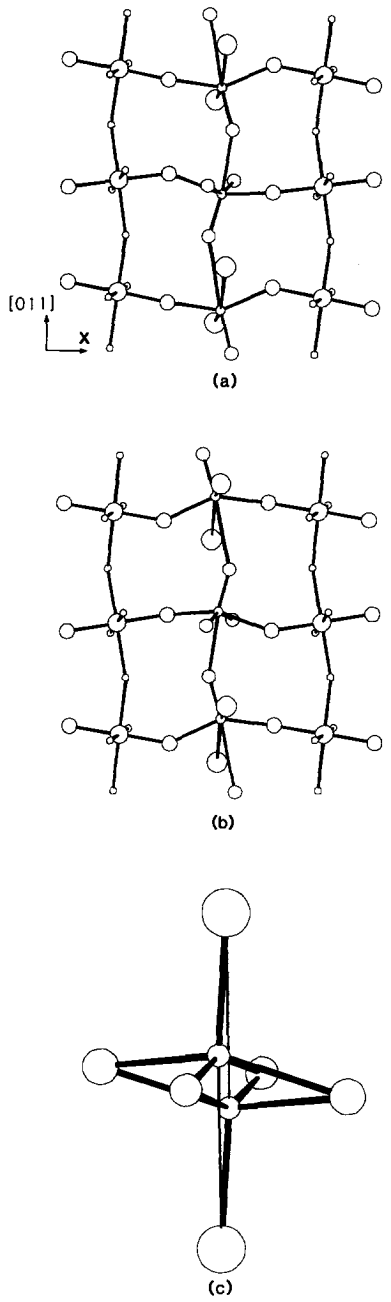

FIG. 4. A layer in the $(0\bar{1}1)$ plane showing the environment about the half-occupied Mo(2) sites near (a) (1/2, 1, 0.1) and (b) (1/2, 1, −0.1). The Mo(2) adjusts its position within the octahedron of oxygen atoms to form a short Mo=O bond. This geometry is also observed in β'-MoO_3 (*3*). This is a simplified example in which only half of the available sites for the O(3) and O(4) atoms have been used in order to emphasize the displacements of the Mo(2) atom from its ideal position at (1/2, 0, 0). The relationship between the two half-occupied sites within this octahedron is shown in (c). See text and Fig. 5 for more details.

tion $\Delta d/d$ of 1×10^{-3}. Data were collected in four detector banks, at approximately 148° and 90°, for about 24 hr at average proton currents on the spallation source of 50 μA. Some of the diffraction data collected in the 90° banks are shown in Fig. 3.

Part of this same sample was also used for the collection of X-ray diffraction data at the X-7A beamline at the National Synchrotron Light Source (NSLS), Brookhaven National Laboratory. The beamline was configured in the high resolution mode (*6*), using a Si(111) monochromator and Ge(220) analyzer. The wavelength, calibrated using an Si powder standard with $a = 5.430825$ Å, was 1.29600(5) Å.

3. Results and Discussion

3.1. Structure Determination

Perusal of both the neutron and the X-ray powder diffractograms indicated that all peaks could be explained by either the monoclinic unit cell with space group $P2_1/c$, published for β-MoO_3 (*3*, *4*), or by the orthorhombic *Pbnm* cell, published for α-MoO_3 (*1*). Particular attention was paid to those portions of the pattern where absences in space group $P2_1/c$ ($h0l$, $l = 2n + 1$ and $0k0$, $k = 2n + 1$) would be expected to occur. No evidence of a lower symmetry was found.

The X-ray and neutron powder diffraction (Fig. 3) patterns showed characteristics of the pseudocubic 3.9-Å cell, suggestive of a perovskite-type structure, in agreement with the conclusions of McCaron in his initial description (*2*) of this form of MoO_3. A

TABLE I

REFINED ATOMIC POSITIONAL[a] AND THERMAL PARAMETERS (Å^2) FOR β-MoO_3 ($P2_1/c$, a = 7.1228(7), b = 5.3660(6), c = 5.5665(6)Å, β = 92.01(1)°

Atom	Site	x	y	z	U × 10^2
Mo(1)	$\bar{1}$	0	0	0	6.9(4)
Mo(2)	1(1)[b]	0.4975(12)	0.9804(15)	0.1146(15)	1.7(2)
O(1)	1	0.9611(8)	0.2837(10)	0.2124(9)	1.2(2)
O(2)	1	0.2447(17)	0.0794(8)	0.9982(12)	4.7(2)
O(3)	1[b]	0.5339(25)	0.2996(27)	0.9288(30)	9.4(7)
O(4)	1[b]	0.5572(20)	0.2828(27)	0.7630(21)	4.3(4)

Note. Final discrepancy indices (*7*) are R_N = 0.088, R_{wp} = 0.077, R_p = 0.057, χ^2 = 3.7. Numbers in parentheses refer to the estimated standard deviation (e.s.d.) for that parameter.

[a] Refinement of the scale factors indicates the β-phase constitutes 85 mole% of the sample.

[b] Split sites with half occupancy. The full symmetry sites from which these are derived are given in parentheses.

Patterson map, calculated using intensities from the β-phase, which had been extracted from the X-ray powder diffraction pattern, was consistent with two possible models for the positions of Mo in the structure. With reference to the space group $P2_1/c$, these are: (a) one Mo at the general position (site symmetry 1) close to (1/4,0,0), and (b) two Mo at inversion centers $\bar{1}$ at (0,0,0) and (1/2,0,0). The oxygen atom positions can be calculated assuming an ReO_3-related structure.

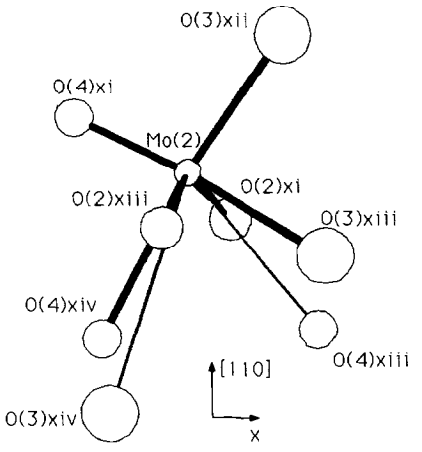

FIG. 5. The environment about Mo(2) showing those O-sites within 1.6 to 3.5 Å. The view is roughly along the O(2)–Mo(2)–O(2) bond with the Mo(2)–O(3) and Mo(2)–O(4) vectors being approximately in the plane of the paper. Valence sums (*8*) suggest that, for this half-occupied Mo(2) site, the sites O(3)xiii and O(4)xiv are occupied rather than O(3)xiv and O(4)xiii.

Calculation of the powder diffraction patterns, based upon the two possible models, suggested the structure containing five independent atoms, Mo(1) at (0,0,0), Mo(2) at (1/2,0,0), and three independent oxygen atoms close to (0,1/4,1/4), (1/4,0,0), and (1/2,1/4,3/4), would be the better basis from which to start structural refinement. All computations were carried out using the Generalized Structure Analysis System (GSAS) of programs (*7*) and these confirmed the correctness of a structure based upon a corner-linked array of MoO_6-octahedra.

For the initial refinements the atomic parameters of the contaminant phase, α-MoO_3, were fixed at those values given in the literature (*1*); only the scale factor for this phase was refined and indicated the α-phase constituted 15 mole% of the sample. The positional and thermal parameters for the Mo and O sites in β-MoO_3 were varied. The large values for the thermal parameters obtained from these refinements prompted

the calculation of Fourier difference maps based upon the intensities extracted from the observed pattern (*7*). These revealed the presence of significant amounts of disordering of the Mo(2) and the O(3) sites, for which the nuclear density was found to be elongated parallel to the *c*-axial direction. In order to model these features, the Mo(2) was displaced, from the center of symmetry at (1/2,0,0), to a general position with half occupancy. The O(3) atom was also distributed over two partially occupied sites, designated O(3) and O(4) in Table I. Refinement of the positional and thermal parameters decreased the discrepancy between the observed and calculated neutron powder diffraction patterns from a goodness-of-fit (χ-square) index of 7.8 for the model containing fully occupied sites at ideal positions, to a value of 4.5 for the disordered model. As an alternative to the use of split-atoms as models for the observed distribution of density in the Fourier difference maps, anisotropic thermal parameters were varied for fully occupied sites on the ideal positions. As expected, these showed large values for U_{33}, the component of the thermal-motion probability ellipsoid along the *z*-axis. No improvement in the χ-square value was observed for these refinements with respect to refinements where split sites were used. Since the split atom model involved the use of fewer parameters to describe the structure, it was adopted for the remaining refinements.

The thermal parameters of some of the remaining atoms were also large (see Table I) and suggestive of further disorder. However, the addition of more split atom sites and parameters to the refinement added little in terms of improvement to the overall fit to the observed data. It added even less in terms of the interpretation of a chemically reasonable model for this material.

At this stage the profile fitting parameters (*7*) were examined. Several peaks were observed to be broadened with respect to the remainder of the pattern. An anisotropic peak broadening term was included in the peak description (*7*); by trial and error, [10$\bar{2}$] was determined to be the preferred broadening direction. It is interesting to note that this corresponds to the direction along which a structure of the ReO_3-type might shear in order to produce the α-form of MoO_3 (Fig. 1).

The results of the final refinement cycles, in which the ratio of parameter shifts to standard deviation were <0.01, are given in Fig. 3 and Table I. Attempts to vary all structural and thermal parameters, for both the α- and β-phases, as well as profile parameters, led to unstable refinements and the type of slow convergence suggestive of strong correlations between parameters. Despite the possibility that α-MoO_3, produced in the fashion described here, may be a disordered variant of the structure given in the literature (*1*), we thought it prudent to fix its positional and thermal parameters. Selected bond lengths and angles for the β-phase are given in Tables II and III, respectively.

TABLE II

SELECTED INTERATOMIC DISTANCES (Å) FOR β-MoO_3

Atoms	Distance (Å)	Atoms	Distance (Å)
Mo(1)—O(2)i	1.795(12)	Mo(2)—O(4)xi	1.622(17)
—O(2)ii	1.795(12)	—O(2)xiii	1.965(15)
—O(1)iii	1.953(5)	—O(2)xi	1.987(15)
—O(1)iv	1.953(5)	—O(3)xiii	2.022(20)
—O(1)v	1.989(5)	—O(3)xii	2.119(24)
—O(1)vi	1.989(5)	—O(4)xiv	2.374(17)
		—O(4)xiii	2.589(13)
Mo(2)—Mo(1)vii	3.580(10)	—O(3)xv	2.737(17)
—Mo(2)viii	3.077(8)	—O(3)xiv	3.177(17)
—Mo(2)x	3.077(8)		

Note. Roman numerals refer to the unit cell transformations: (i) $x, y, z - 1$; (ii) $-x, -y, 1 - z$; (iii) $x - 1, y, z$; (iv) $1 - x, -y, -z$; (v) $1 - x, y - 1/2, 1/2 - z$; (vi) $x - 1, 1/2 - y, z - 1/2$; (vii) $x, 1 + y, z$; (viii) $1 - x, y - 1/2, 1/2 - z$; (ix) $1 - x, 2 - y, -z$; (x) $1 - x, 1/2 + y, 1/2 - z$; (xi) $1 - x, 1 - y, 1 - z$; (xii) $x, 3/2 - y, z - 1/2$; (xiii) $x, 1 + y, z - 1$; (xiv) $1 - x, 1/2 + y, 1/2 - z$; (xv) $1 - x, 1/2 - y, 3/2 - z$.

TABLE III

SELECTED INTERATOMIC ANGLES[a] (°) FOR β-MoO_3 AND DISTANCES[a] (Å) BETWEEN OXYGEN ATOMS INVOLVED IN THE ANGLE

Atoms	Distance	Angle	Atoms	Distance	Angle
O2i—Mo1—O2ii	3.59	180.0	O4ix—Mo2—O2viii	2.72	98.2
—O1iii	2.62	88.6	—O2xi	2.84	103.3
—O1iv	2.68	91.3	—O3xiii	3.63	171.7
—O1v	2.72	92.0	—O3xii	2.87	99.4
—O1vi	2.63	88.0	—O4xiv	2.80	87.0
O2ii—Mo1—O1iii	2.68	91.3	—O4xiii	4.12	155.8
—O1iv	2.62	88.6	—O3xiv	3.74	97.1
—O1v	2.63	88.0	O2viii—Mo2—O2xi	3.73	141.8
—O1vi	2.72	92.0	—O3xiii	2.42	74.6
O1iii—Mo1—O1iv	3.91	180.0	—O3xii	3.17	101.8
—O1v	2.77	89.2	—O4xiv	2.60	73.1
—O1vi	2.81	90.8	—O4xiii	2.84	75.8
O1iv—Mo1—Ov	2.81	90.8	—O3xv	3.82	107.3
—O1vi	2.77	89.2	—O3xiv	3.26	74.7
O1v—Mo1—O1vi	3.98	180.0	O2xi—Mo2—O3xiii	2.60	80.7
			—O3xii	3.26	105.3
O3xi—Mo2—O4xii	3.03	155.7	—O4xiv	2.73	77.0
—O2xiii	2.60	94.9	—O4xiii	2.72	71.6
—O2xi	2.42	85.6	—O3xv	3.90	110.0
—O3xiii	3.35	140.2	—O3xiv	3.17	71.6
—O3xii	3.36	133.4	O3xiii—Mo2—O3xii	2.83	86.3
—O4xiii	3.63	121.4	—O4xiv	3.03	86.9
—O3xv	2.83	77.5	—O3xv	4.51	142.3
—O3xiv	2.83	63.1	—O3xiv	3.36	77.2
O4xii—Mo2—O4xi	2.81	123.3	O3xii—Mo2—O4xiv	4.48	172.4
—O2xiii	2.73	100.5	—O4xiii	3.74	104.8
—O2xi	2.60	93.5	—O3xv	2.35	56.1
—O4xiv	3.81	149.6	—O3xiv	5.24	163.5
—O4xiii	2.80	80.9	O4xiv—Mo2—O4xiii	2.806	68.7
—O3xv	2.91	80.0	—O3xv	4.64	130.4
—O3xiv	4.48	139.3	O4xii—Mo2—O3xv	5.25	160.9
			—O3xiv	2.87	58.6
			O3xv—Mo2—O3xiv	5.57	140.4

[a] Roman numerals refer to the unit cell transformations given in the footnote to Table II. The estimated standard deviations in the O–O distances and Mo–O–Mo angles are 0.02 Å and 0.7°, respectively.

3.2. Comparison of β-MoO_3 with α- and β'-MoO_3

The structures of α-, β- and β'-MoO_3 are compared in Figs. 1 and 2 where the idealized positions for Mo(2), O(3), and O(4) have been used. The partial occupancy of the Mo(2)-, O(3)-, and O(4)-sites in the *average* structure of β-MoO_3, is a consequence of the tendency of Mo to favor distorted octahedral environments (*1*). In both the α- and β-forms of MoO_3, short Mo–O interatomic distances (<1.7 Å) have been observed (*1, 3*). Kihlborg (*1*) pointed out that the coordination of Mo by oxygen in α-MoO_3 is intermediate between tetrahedral

and octahedral. This feature is also observed in β'-MoO_3 (*3*). Rather than form six bonds of equal strength with oxygen, Mo in MoO_3 tends to form a distribution, best described[1] as 2 + 2 + 2 in the case of α-MoO_3 and 1 + 3 + 2 for β'-MoO_3 (*3, 9*). The distribution of distances around the disordered Mo(2) atom can be interpreted as resulting from the formation of a short bond, directed either in [011] or [$0\bar{1}\bar{1}$], as shown in Figs. 4 and 5.

Although the interpretation of the structure of β-MoO_3 is complicated by the disorder described above, a reasonable model for the oxygen atoms coordinated to Mo(2) can be proposed based upon the calculated bond valence (*8*). In Table II all distances less than 3.5 Å from Mo(2) are given. The O(2)-sites are fully occupied and the remaining four oxygens required to complete the distorted octahedral coordination about Mo(2) must be chosen from the sites populated by O(3) and O(4); since these are half occupied, on average, an equal number of O(3) and O(4) sites make up the Mo(2) coordination sphere. If very short bonds (<1.6 Å) are eliminated on the basis that no such distances are observed in the other forms of MoO_3 (*1, 3*), then the possible sites shown in Fig. 5 are obtained. Two sets of closely spaced O(3) and O(4) sites (Table III) are shown at the bottom of the drawing. The likelihood of occupancy of these two sets of sites can be assessed on the basis of the valence sums about Mo(2). These sums for Mo in both the α- and the β'-forms of MoO_3, calculated in accordance with the empirical formulae given by Brown (*8*), are close to 6, as would be expected for Mo^{6+}. For α-MoO_3 the value is 5.9 and for β'-MoO_3 it is 6.2 and 6.0 for the two independent sites occupied by Mo in this structure. For the Mo(1) site in β-MoO_3, the valence sum if 5.7. For the Mo(2) site, the valence sum is 5.5 when the shorter distances to O(3) and O(4) are included in the calculation; it is 4.8 when the longer distances are included.

Given the degree of disorder, there are a number of plausible interpretations of the structure. However, the interpretation given above accords with the known structures of the other polymorphs of MoO_3, and the tendency for octahedrally coordinated Mo to form one or two short bonds with O.

[1] Only in a few instances, such as the ordered perovskites, $A_2^{II}B^{II}MoO_6$, are regular Mo(VI) octahedra observed. The notation refers to the number of short (molybdenyl, Mo=O) bonds, intermediate (roughly single) bonds, and long (fractional) bonds, making up the distorted octahedron: (s + i + l). In the case of (3 + 3) there are 3s and 3l. See also Ref. (*9*).

Acknowledgments

J.B.P.is grateful to the DuPont company for providing some of the funds expended during this work. LANSCE is operated under U.S. Government Contract W-7405-ENG-36. Work at beamline X-7A at the NSLS was supported under DOE Contract DE-ASO5-80-ER10742.

References

1. B. G. HYDE, AND S. ANDERSON, "Inorganic Crystal Structures" pp. 14, 20, 373, Wiley Interscience, (1989); for α-MoO_3 see also KIHLBORG, L. *Arkiv Kemi* **21,** 357 (1963).
2. E. M. MCCARRON III, *J. Chem Soc. Chem. Commun.*, 336 (1986).
3. J. B. PARISE, E. M. MCCARRON, AND A. W. SLEIGHT, *Mater. Res. Bull.* **22,** 803 (1987).
4. L. GANAPATHI, A. RAMANAN, J. GOPALAKRISHANAN, AND C. N. R. RAO, *J. Chem. Soc. Chem. Commun.*, 62 (1986); F. HARB, B. GERAND, G. NOWOGROCKI, AND M. FIGLARZ, *C.R. Acad. Sc. Paris, Ser. II* **303,** 349 (1986); G. SVENSSON AND L. KIHLBORG, *React. Solids* **8,** 33 (1987).
5. P. F. CARCIA AND E. M. MCCARRON III U.S. Patent 4,753,916, June 28, 1988.

6. D. E. Cox, B. H. Toby, and M. M. Eddy, *Aust. J. Phys.* **41,** 117 (1988).
7. A. C. Larson, and R. B. Von Dreele, "GSAS manual," Los Alamos Report LAUR 86-748 (1986).
8. I. D. R. Brown, *in* "Structure and Bonding in Crystals," Vol. II, (M. O'Keefe and A. Navrotsky Eds.), Vol. II, pp. 1–29, Academic Press, (1981).
9. J. B. Goodenough, "Proceedings of the Climax 4th International Conference on the Chemistry and Uses of Molybdenum" (H. F. Barry and P. C. H. Mitchell, Eds.), pp. 1–22, Climax Molybdenum Co., Ann Arbor, MI (1982).